ADVANCED ENERGY & SUSTAINABILITY RESEARCH
Open Access
www.advenergysustres.com

The Influence of Polyethylene Oxide Degradation in Polymer-Based Electrolytes for NMC and Lithium Metal Batteries

*Lukas Herbers, Jaroslav Minář, Silvan Stuckenberg, Verena Küpers, Debbie Berghus, Sascha Nowak, Martin Winter, and Peter Bieker**

A multilayered ternary solid polymer electrolyte (TSPE) is presented. First, the influence of polyethylene oxide degradation on cell failure, development of subsequent volatile degradation products, and cell impedance is analyzed. The low electrochemical stability window/oxidative stability (≥3.8 V) results in side-chain oxidation and loss of active material. Subsequently, electrolyte stability is improved and a thin-film (≤50 µm) TSPE with three functional layers is developed to match the wide-ranging electrolyte requirements toward Li metal anodes and different cathode materials like $LiNi_{0.6}Mn_{0.2}Co_{0.2}O_2$ and $LiFePO_4$ (NCM622, LFP). The high-voltage stability of ≥4.75 V makes the TSPE a promising candidate in high-voltage applications. Because of high Coulombic efficiencies in NMC622‖Li metal (99.7%) and LFP‖Li metal (99.9%) cells, the presented electrolyte enables stable long-term cycling with great capacity retention of 86% and 94%, respectively. The temperature stability of >300 °C and the capability to prevent high surface area Li and dendrite formation (even at an areal capacity utilization of >40 mAh cm^{-2}) contribute to high safety under a wide range of conditions.

1. Introduction

The transition from fossil fuels as primary energy sources to renewable energies leads to a groundbreaking change in the whole industry and the way of energy management in modern societies.[1] The fluctuation in energy availability in the grid by renewable sources and the avoidance of fossil fuels in vehicles require energy-efficient approaches for energy storage.[2,3] Therefore, the demand for batteries is considered to increase massively in the 21st century.[4] Due to a diverse field of stationary and portable battery applications, requirements for batteries are manifold, and high standards for safety, lifetime as well as energy density must be fulfilled.[5] Li-ion batteries are the most used battery type in commercialized automotive and consumer electronics batteries but are limited in regards to specific energy (Wh/kg) in comparison to other systems.[6]

Li metal anodes provide a higher specific capacity of 3860 mAh g^{-1} in comparison to widely used graphite anodes (372 mAh g^{-1}).[7,8] Furthermore, the low standard reduction potential of −3.04 V versus standard hydrogen electrode of Li metal in combination with high voltage cathode materials like lithium nickel manganese cobalt oxides (NMC) makes Li metal an ideal anode material for Li-based battery technologies with high voltage and specific energy.[9,10] Despite its advantages, the application of Li metal electrodes leads to potential safety risks due to the formation of reactive high surface area lithium (HSAL) morphologies, with needle-like (dendritic) morphologies being the most known ones, which can cause internal short circuits and generally increase the risk of thermal runaway.[11] Furthermore, volatile organic liquid electrolytes decrease safety by potential gas evolution and their flammability.[11] To benefit from the high specific energy of NMC‖Li cells and minimize the safety risks of Li metal conventional organic liquid electrolytes can be replaced by solid polymer electrolytes (SPEs).[12,13]

SPEs like polyethylene oxide (PEO) combined with a Li salt, like lithium bis(trifluoromethanesulfonyl)imide (LiTFSI), are considered safer because 1) the solid-state avoids electrolyte leakage; 2) the high melting and boiling points and/or decomposition temperature minimize volatility; and 3) of the low flammability reduces the risk of ignition.[14] Nonetheless, polymer electrolytes

L. Herbers, J. Minář, S. Stuckenberg, V. Küpers, D. Berghus, S. Nowak, M. Winter
MEET Battery Research Center
Institute of Physical Chemistry
University of Münster
48149 Münster, Germany

M. Winter, P. Bieker
Helmholtz-Institute Münster (HI MS)
IEK-12
Forschungszentrum Jülich GmbH
48149 Münster, Germany
E-mail: peter.bieker@uni-muenster.de

The ORCID identification number(s) for the author(s) of this article can be found under https://doi.org/10.1002/aesr.202300153.

© 2023 The Authors. Advanced Energy and Sustainability Research published by Wiley-VCH GmbH. This is an open access article under the terms of the Creative Commons Attribution License, which permits use, distribution and reproduction in any medium, provided the original work is properly cited.

DOI: 10.1002/aesr.202300153

© 2023 The Authors. Advanced Energy and Sustainability Research published by Wiley-VCH GmbH

26999412, 2023, 12, Downloaded from https://onlinelibrary.wiley.com/doi/10.1002/aesr.202300153 by Forschungszentrum Jülich GmbH Research Center, Wiley Online Library on [09/04/2024]. See the Terms and Conditions (https://onlinelibrary.wiley.com/terms-and-conditions) on Wiley Online Library for rules of use; OA articles are governed by the applicable Creative Commons License

also have major drawbacks compared to conventional organic liquid electrolytes. While organic liquids ensure sufficient ion mobility and thereby enable rapid transport of solvated ions, solid polymers are immobilized and only enable ion mobility to a certain extent.[15] In the case of PEO, the Li-ions are complexed by the coordination of ethylene oxide (EO) groups in the polymer chain. Therefore, the Li salt is dissolved in the PEO by ion dissociation, and ions are shuttled through the polymer matrix by rearrangement of the EO chains.[16] As a result, SPEs suffer from a lower ionic conductivity when compared to liquid electrolytes because the long polymer chains are immobile and unable to provide a rapid reorganization.[14]

To enhance mobility of EO chains as well as to ease the rearrangement necessary for ion transport, the PEO can be plasticized by adding liquids to the SPE.[9] To avoid the safety risks of organic solvents, room temperature (RT) ionic liquids (ILs) are considered advantageous.[17] Despite their higher price than organic electrolytes, they have a negligible vapor pressure and are more thermally stable, allowing for maintaining the high safety granted by SPEs.[18] The IL-based SPEs are also referred to as ternary solid polymer electrolytes (TSPE) and consist of three major components (polymer, IL, and Li salt, see **Figure 1**). For example, the addition of the IL 1-butyl-1-methyl-pyrrolidinium-bis-(trifluoromethylsulfonyl)imid ($Pyr_{14}TFSI$) to a PEO-LiTFSI SPE increases the RT ionic conductivity by orders of magnitude.[19]

Despite the advantages of TSPEs, Zhang et al. reported that TSPEs may suffer from low mechanical strength leading to HSAL growth through the electrolyte, increasing the risk of a cell failure by short circuits.[20] They developed a composite TSPE using as Celgard 2500 (Cg) separator with high modulus domain, which is coated with a PEO-based ternary solid polymer electrolyte (→CgPEO). While the TSPE grants a high ion conduction across the Cg, HSAL growth is suppressed by the mechanical strength of the extra CgPEO in comparison to the pure TSPE. Additionally, this approach enabled thin electrolyte films ($\leq$50 µm) to be used in cells with high areal capacity utilization (5 mAh cm^{-2}). Nonetheless, despite the mentioned improvements in regards to ionic conductivity and reduction of safety concerns when cycling a Li metal electrode, also the requirements of electrolytes toward the cathode have to be adjusted.

In this work, the CgPEO electrolyte is further improved to empower enhanced cycling of both the Li metal anode as well as state-of-the-art cathodes containing active materials like NMC622 ($LiNi_{0.6}Mn_{0.2}Co_{0.2}O_2$) or lithium iron phosphate (LFP, $LiFePO_4$). While most components in the TSPE, like $Pyr_{14}TFSI$ and LiTFSI, are considered stable in the applied voltage ranges of NMC622||Li cells (3.00–4.25 V), PEO is slowly oxidized above 3.80 V.[21–23] These parasitic reactions can result in the formation of a thick cathode electrolyte interphase (CEI[24]), increased cell resistance and thereby overvoltage, the loss of active Li by NMC degradation, and the formation of volatile small-chain PEO decomposition products, causing a potential safety risk.[25]

To minimize electrolyte degradation on the cathode side, Cg-reinforced multilayer electrolytes (CgPVDF, CgPVDF+) are presented in this work. They were manufactured by coating two different ternary electrolytes on each side of a Cg separator to address the different electrochemical stability requirements of the anode and cathode (see **Figure 2**a,b).[26] A cross-linked PEO-based ternary electrolyte is used facing the anode side,

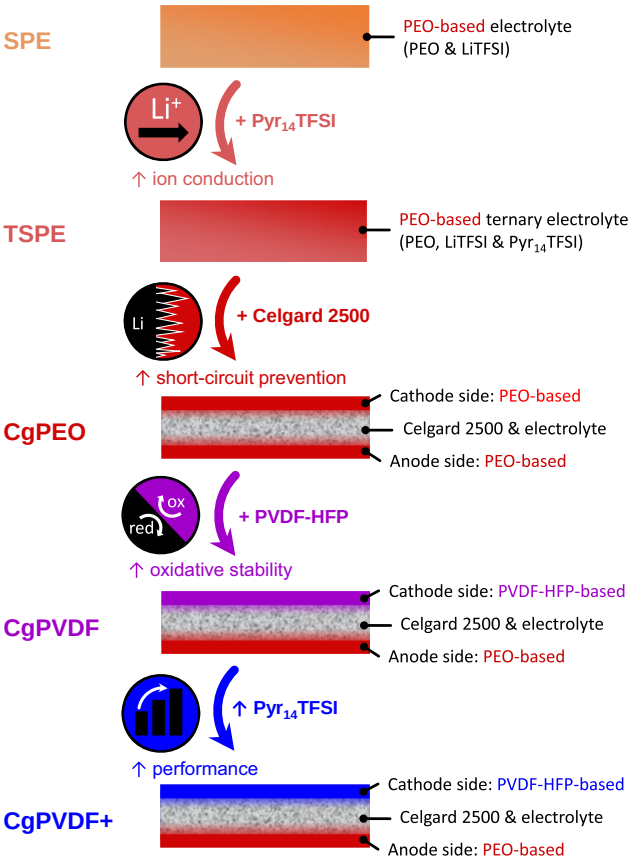

Figure 1. Evolution of ternary electrolytes in this work. Improvement of electrolyte properties by addition of $Pyr_{14}TFSI$, Celgard 2500, PVDF-HFP, and increase in $Pyr_{14}TFSI$ ratio. Electrolytes sketch from top to bottom: solid polymer electrolyte (SPE), ternary solid polymer electrolyte (TSPE), Celgard 2500 coated with a PEO-based ternary solid polymer electrolyte (CgPEO), and Cg-reinforced multilayer electrolytes (CgPVDF, CgPVDF+).

providing great connectivity toward Li metal and high ion conduction. To improve the oxidation stability of the electrolyte facing the cathode side, PEO in the ternary electrolyte is replaced by an equivalent mass of poly(vinylidene fluoride-co-hexafluoropropylene) (PVDF-HFP) as a more oxidation-stable polymer (see Figure 2c).[27,28] A cross-section of the CgPVDF+ electrolyte is shown in the Supporting Information, see Figure S1, Supporting Information.

The transition from a PEO-based CgPEO to an improved multilayer CgPVDF+ is analyzed and discussed. First, the influence of PEO degradation at high cell voltages is analyzed and the positive effects of implementing PVDF-HFP in this regard are discussed. Second, the composition of the PVDF-HFP-based CgPVDF is optimized for electrochemical performance and the long-term cycling stability of the resulting CgPVDF+ is shown.

1.1. Chemicals

PEO (Dow Chemical, molecular weight 4 000 000) was dried at 60 °C for at least 48 h under reduced pressure $\leq 10^{-3}$ mbar, followed by 48 h at 60 °C under reduced pressure $\leq 10^{-7}$ mbar.

© 2023 The Authors. Advanced Energy and Sustainability Research published by Wiley-VCH GmbH

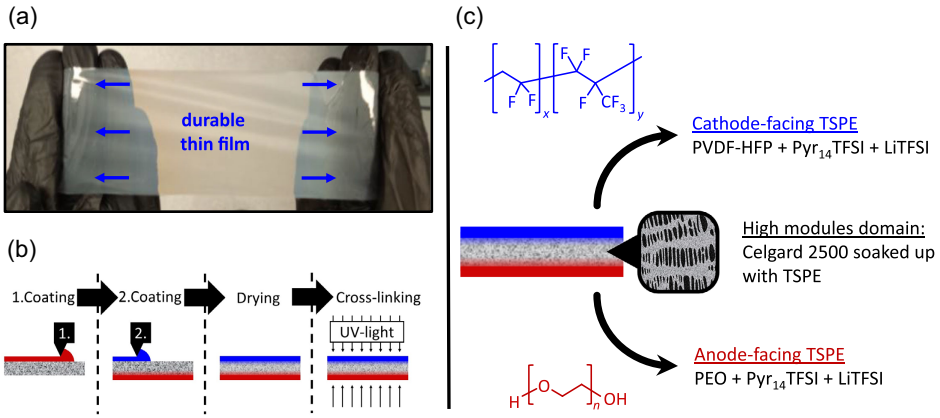

Figure 2. Electrolyte processing and design. a) Top view of a stretched 50 µm-thick CgPVDF+ electrolyte; b) processing of multilayer electrolytes by 1. coating, 2. coating, drying, and cross-linking; c) sketch of the side view of a CgPVDF+ electrolyte.

Benzophenone (BP) (Merck, 99%), acetonitrile (ACN) (Carl Roth, ≥99.9%, ROTIDRY, ≤10 ppm H_2O), and 1-methyl-2-pyrrolidinone (NMP) (Thermo Fisher Scientific, 99.5%, AcroSeal, over molecular sieve) were used as received. $Pyr_{14}TFSI$ (Solvionic, 99.9%), LiTFSI (TCI, >98%) and PVDF-HFP (Sigma-Aldrich, molecular weight 400 000) were dried for at least 48 h at 110 °C under reduced pressure $\leq 10^{-3}$ mbar, followed by 48 h at 110 °C under reduced pressure $\leq 10^{-7}$ mbar. NMC622 sheets (experimental capacity 180 mAh g^{-1}) and LFP sheets ($LiFePO_4$, NANOMYTE BE-60E, experimental capacity ≥170 mAh g^{-1}, NEI Corporation) were dried for 48 h at 100 °C under reduced pressure $\leq 10^{-3}$ mbar.

1.2. Preparation

The electrolyte films were prepared in a dry room, as described by Zhang et al.[20] The PEO-based electrolytes were prepared by dissolving PEO, LiTFSI, $Pyr_{14}TFSI$, and BP in ACN (0.22 g PEO per 10 mL ACN). The PVDF-HFP electrolytes were prepared by dissolving PVDF-HFP, LiTFSI, and $Pyr_{14}TFSI$ in NMP (1.67 g PVDF-HFP per 10 mL NMP). A molecular ratio of 10:2:1:0.12 (EO:$Pyr_{14}TFSI$:LiTFSI:BP) for CgPEO, a molecular ratio of 10:2:1 ($EO_{equiv.}$:$Pyr_{14}TFSI$:LiTFSI) in which PEO was replaced by an equivalent mass of PVDF-HFP for CgPVDF and a molecular ratio of 10:4:1 ($EO_{equiv.}$:$Pyr_{14}TFSI$:LiTFSI) for CgPVDF+ was used for the electrolytes. CgPEO/CgPVDF (50:50) was prepared by preparing a 50:50 mixture of CgPEO and CgPVDF in NMP. The electrolyte pastes were applied using a doctor blade. One side of the Cg was coated with the PEO-based paste and dried in the dry room (relative humidity ≤0.05%). Afterward, the second side of the Cg was coated with the PVDF-HFP-based paste and dried at 60 °C under reduced pressure $\leq 10^{-3}$ mbar for 48 h. The membranes were cross-linked from both sides by UV curing (UVACUBE 100, 100 W lamp, Dr. Hönle AG) for 10 min. The process is summarized in Figure 2b.

Electrochemical measurements were conducted in CR2032 two-electrode cells, which were assembled with two electrode discs (12 mm diameter) in stainless steel (SST)||Li, symmetric Li||Li, LFP||Li, and NMC622||Li cells in a dry room. All measurements were performed at 60 °C. Linear sweep voltammetry (LSV) measurements (0.5 mV s^{-1}, from open circuit voltage (OCV) to 5.6 V) were obtained in SST||Li cells and single charge measurements (0.05 mA cm^{-2} from OCV to 4.00, 4.25, 4.50, 4.75, or 5.00 V) in NMC622||Li metal cells. The long-term electrochemical cycling stability (0.05 mA cm^{-2}, 1 h OCV before and after impedance measurement after each cycle, 10 mHz to 1 MHz) was performed in NMC622||Li metal cells. The galvanostatic discharge polarization (0.10 mA cm^{-2}) in symmetric Li||Li cells, charge pulse measurement/amperometry for limiting diffusion current rate determination (≥0.8 mA cm^{-2}, cut-off voltage 1 V) in symmetric Li||Li cells, and voltammetry for limiting diffusion current rate determination (0.01 mA cm^{-2}) in were obtained in symmetric Li||Li cells. All these electrochemical measurements were performed on a VMP potentiostat (Bio-152 Logic). Galvanostatic polarization studies (0.10 mA cm^{-2}, 2.5–4.0 V) with LFP||Li metal cells and galvanostatic polarization studies (0.10 mA cm^{-2}, 3.0–4.25 V) with NMC622||Li cells were performed on a MACCOR battery cycler (MACCOR Series 4000).

The temperature stabilities of the electrolytes were studied using thermogravimetric analysis (TGA, A Q5000IR by TA instruments) with a heat rate of 10 K min^{-1} from 30 to 600 °C under nitrogen.

Fourier-transform infrared spectroscopy (FT-IR) measurements were performed on a BRUKER ALPHA II. The samples were placed on the attenuated total reflection crystal and a wavenumber range from 1900 to 1525 cm^{-1} was measured.

The samples for solid-phase microextraction gas chromatography-mass spectrometry measurements (SPME-GC-MS) were prepared by disassembling coin cells in a dry room and transferring the solid electrolyte and cathode into separate 20 mL headspace vials. GC-MS measurements were carried out using Shimadzu QP2010 Ultra single quadrupole (SQ), equipped with AOC-5000 autosampler. For the sample extraction, a divinylbenzene-polydimethylsiloxane fiber (65 µm, Restek) was exposed to the headspace for 10 s at RT to prevent thermal decomposition of solid polymer electrolytes. The analytes were further desorbed in the heated split-splitless injection unit (250 °C) of GC for 1 min at a split of 1:10. The compound identification was validated with NIST 11 and by comparison of mass spectrum and retention time with analytical standard. The measurement was performed as

© 2023 The Authors. Advanced Energy and Sustainability Research published by Wiley-VCH GmbH

26999412, 2023, 12, Downloaded from https://onlinelibrary.wiley.com/doi/10.1002/aesr.202300153 by Forschungszentrum Jülich GmbH Research Center, Wiley Online Library on [09/04/2024]. See the Terms and Conditions (https://onlinelibrary.wiley.com/terms-and-conditions) on Wiley Online Library for rules of use; OA articles are governed by the applicable Creative Commons License

described elsewhere.[29] The SPME fiber was conditioned after each measurement at 260 °C for 5 min and was checked by blank measurement.

2. Results and Discussion

2.1. Oxidative Stability of CgPEO versus CgPVDF

As will be discussed in this work, at high potentials PEO suffers from oxidative degradation toward the cathode–electrolyte interface which comes along with NMC capacity fading by active material reduction.[25,30,31] This redox reaction has multiple causes, which diminish cell capacity and shorten the longevity of the battery. The following effects are of interest: 1) loss of active material by rock salt generation, 2) formation of volatile degradation products, 3) NMC corrosion by the formation of HTFSI, 4) increase in cell resistance e.g., through CEI formation, and 5) PEO degradation by ester formation and chain scission (see **Figure 3**).

The voltage range in which the electrolyte remains stable is often expressed by the electrochemical stability window (ESW). At voltages outside the ESW, the electrolyte is reduced (reductive stability at lower ESW) or oxidized (oxidative stability at the upper ESW). Especially the oxidative stability is of interest to understand the compatibility of an electrolyte toward high voltage cathode materials.

To analyze the oxidative stability of an electrolyte, the LSV technique can be used. Hereby the electrolyte is sandwiched between a Li metal electrode and a blocking auxiliary electrode like a SST electrode, see **Figure 4**c(i). The voltage between the electrodes is increased with a constant scan rate (0.5 mV s^{-1}) while the current is monitored. Because the SST interface is considered electrochemically inactive, no major current is observed unless the electrolyte is stable. Only a steady low increase in current is observed due to ion migration within the electrolyte in the low voltage region, see Figure 4a,c(ii).[30] As soon as the ESW of the electrolyte is exceeded, a current response will be noticeable indicating an electron transfer between cathode and anode, see Figure 4a,c(iii). This is caused by electrolyte oxidation at the SST interface and a simultaneous reduction reaction at the Li metal interface by Li deposition.

An abrupt current increase is notable in all samples from ≈5 V, indicating the upper limit of the ESW with threshold currents of 10 µA cm^{-2} at 4.93 V (CgPEO), 5.21 V (CgPEO/CgPVDF (50:50)) and 5.28 V (CgPVDF) indicating a high oxidation stability for both CgPEO and CgPVDF. However, the upper ESW can be overestimated by only considering the high currents of ≥10 µA cm^{-2}. In the low current region, the upper ESWs of the electrolytes differ visibly, see Figure 3b. For cell voltages ≥3.8 V, the cell containing CgPEO shows a higher current response compared to the cell with CgPVDF, indicating a degradation of PEO.[21,22] At low voltages PEO, is oxidized to form terminal carboxyl groups (≥4.05 V in NMC532‖Li[31]) and ester groups (≥3.9 V in $LiCO_2$‖Li[30]), while at higher voltages, PEO is degraded by chain scission (4.5 V in $LiCO_2$‖Li[25]), forming volatile degradation products. As shown in Figure 4b, the current in SST‖Li cells is reduced (at 4.5 V currents of 7.0 µA cm^{-2} for CgPEO and 1.1 µA cm^{-2} for CgPVDF) by increasing the PVDF-HFP content of the TSPE at the cathode-side.

In summary, the current response at <5 V is likely related to PEO degradation at the cathode side of the electrolyte. A replacement by PVDF-HFP enables a higher voltage stability of up to 4.75 V (≤1.5 µA cm^{-2}) for CgPVDF, making it applicable toward high-voltage cathode materials of the 4 V category. The results are further supported by voltage stability measurements using delithiated active cathode material (Figure S3, Supporting

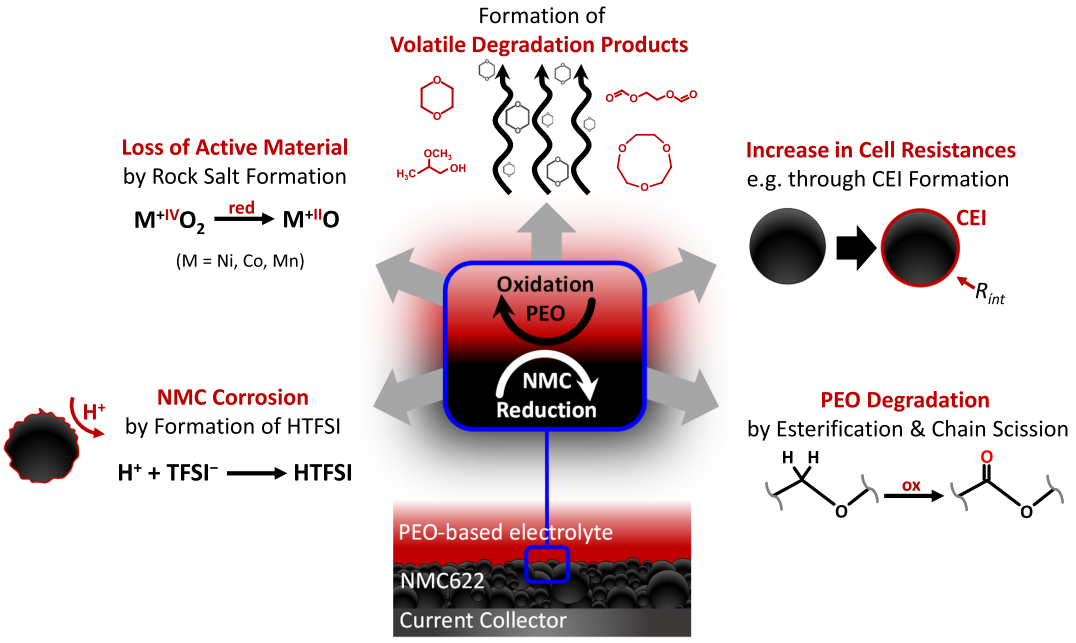

Figure 3. Illustration of the consequences of PEO oxidation and NMC reduction at the PEO-NMC interface.

© 2023 The Authors. Advanced Energy and Sustainability Research published by Wiley-VCH GmbH

26999412, 2023, 12, Downloaded from https://onlinelibrary.wiley.com/doi/10.1002/aesr.202300153 by Forschungszentrum Jülich GmbH Research Center, Wiley Online Library on [09/04/2024]. See the Terms and Conditions (https://onlinelibrary.wiley.com/terms-and-conditions) on Wiley Online Library for rules of use; OA articles are governed by the applicable Creative Commons License

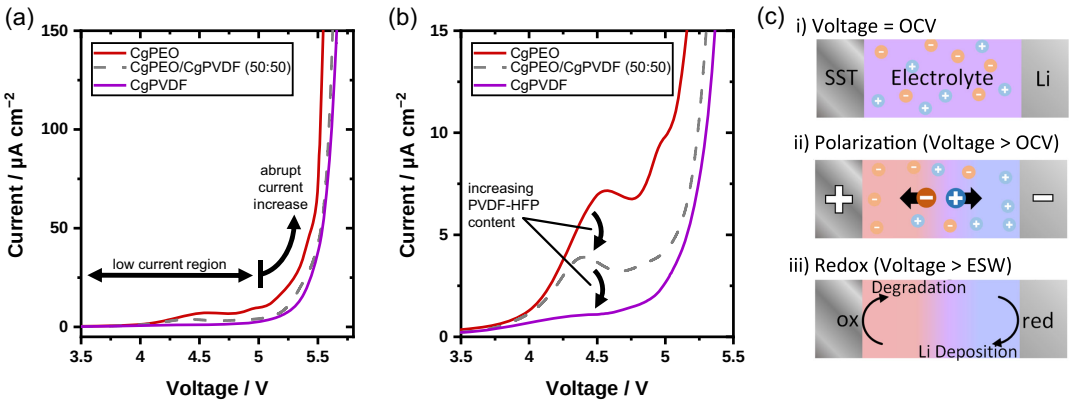

Figure 4. LSV of CgPEO and CgPVDF in SST||Li metal cells with a sweep rate of 0.5 mV s^{-1} at 60 °C. a) LSV from 3.5 to 5.8 V; b) enlargement of figure with a current ≤15 µA cm^{-2}; c) processes during LSV.

Information). Additionally, the results highlight that even low current responses are not negligible for determining the ESW. This agrees with the conclusion made by Cabañero et al. who reviewed the oxidative stability of PEO/LiTFSI electrolytes determined by LSV.[27] The results varied in a wide range from 3.8 up to 4.9 V. As a root cause for the broad span they assumed the subjective choice of the onset point of degradation in the LSV curves. If all current responses before the abrupt current increase (≈5 V) are neglected, the oxidative stability can be overestimated.

To determine the oxidative degradation of CgPEO, NMC622||Li cells are swept with a constant current (0.05 mA cm^{-2}) in a linear sweep amperometry (LSA) or single charge measurement, see **Figure 5**a. LSA is applied with different upper cut-off voltages in a range from 4.00 to 5.00 V and kept at this voltage for 2 h. With higher cut-off voltage, the cathode material is delithiated increasing the specific capacity and the state of charge (SOC) of the NMC622. Furthermore, the PEO is exposed to a stronger oxidative environment at the cathode interface caused by two driving forces. First, as discussed previously, when the voltage exceeds the upper limit of the ESW of 3.8 V of CgPEO, the rate of electrolyte decomposition increases rapidly. Second, during charging/delithiation of NMC622, the metal (III)-oxides in ($LiM^{+III}O_4$, M=Ni, Co, Mn) convert into metal (IV)-oxides ($M^{+IV}O_2$), which are all strong oxidation agents providing a chemical driving force for electrolyte oxidation. After LSA experiment, the cells are disassembled and the electrolyte degradation is analyzed optically, by FT-IR and SPME-GC-MS.

All electrolytes showed a color change to yellow to some degree (see Figure 3b), indicating polymer degradation even at low voltages. Hereby, the intensity of color increases slightly from 4.00 to 4.50 V, followed by turning completely brown for cut-off voltages >4.50 V. This effect is also reflected in FT-IR measurements, which indicates the formation of ester C=O groups after LSA with the characteristic bands at 1642 and 1729 cm^{-1}.[30] The bands intensify with an increased cut-off voltage supporting the severe visible oxidation. Furthermore, the 1729 cm^{-1} band shows a side shoulder at 1740 cm^{-1} for cut-off voltages >4.50 V, which could be related to an even more severe oxidation and the formation of carboxylic acids or carbonates, the C=O stretching band is shifted in comparison to esters. In comparison, no degradation is observed for CgPVDF and CgPVDF+, compare Figure S9, Supporting Information. In addition, the PEO degradation is further evaluated by SPME-GC-MS. Four volatile decomposition products are identified: 1,4-dioxane, 2-methoxy-1-propanol, 1,2-ethylene glycol diformate, and 1,3,6-trioxocane, see Figure 3 and S2, Supporting Information. The main volatile decomposition product 1,4-dioxane, known to be formed upon PEO oxidation, is monitored.[32,33] With increasing cut-off voltage, the amount of 1,4-dioxane increases exponentially from 4.00 to 4.50 V, see Figure 4e. Different from the C=O group formation, the amount of 1,4-dioxane remains at comparable levels from 4.50 V, indicating most of the volatile species is formed by sweeping to 4.50 V with a 2 h hold.

It also has to be noted that the cells with a cut-off voltage >4.50 V show intensive degradation and cell failure at ≈4.6 V, which could potentially limit the amount of degradation occurring above this voltage, see Figure 3a. The cell failure is visible in the LSA curves by a voltage drop caused by increased cell resistances as well as a current flow from electrolyte degradation. The strong electrolyte degradation is most likely a result of two amplifying effects. First, as shown, CgPEO is oxidized when the voltage exceeds the ESW, and the oxidation is accelerated with increasing voltage. As Nie et al. showed in their work, at ≈4.50 V versus Li|Li^+ the degradation of PEO/LiTFSI electrolytes (without $Pyr_{14}TFSI$) is intensified causing severe PEO chain scission.[25] Second, the degradation of the electrolyte cannot be viewed as a single phenomenon, instead, the electrons transferred from oxidative degradation simultaneously can lead to a reduction reaction. As shown by Homann et al. the reduction of Li^+ to Li metal to form dendritic HSAL can potentially lead to a short circuit.[34] For the electrolytes presented in this work, HSAL formation is noncritical, because as will be shown later the implementation of Cg prevents short circuits. A much more severe redox reaction takes place between the electrolyte (oxidized) and the cathode material (reduced), see Figure 5. During charging, the strong oxidant $M^{+IV}O_2$ is formed in NMC622. Furthermore, as reported by Jung et al. NMC622 is nonstable when exceeding a SOC of ≈81% at ≈4.6 V of NMC622.[35,36] At high SOC, reactive oxygen (e.g., singlet oxygen) is released from the materials. Both effects can lead to rapid NMC622 reduction by the formation of rock salt as well as electrolyte oxidation. As rock salt does not

© 2023 The Authors. Advanced Energy and Sustainability Research published by Wiley-VCH GmbH

26999412, 2023, 12, Downloaded from https://onlinelibrary.wiley.com/doi/10.1002/aesr.202300153 by Forschungszentrum Jülich GmbH Research Center, Wiley Online Library on [09/04/2024]. See the Terms and Conditions (https://onlinelibrary.wiley.com/terms-and-conditions) on Wiley Online Library for rules of use; OA articles are governed by the applicable Creative Commons License

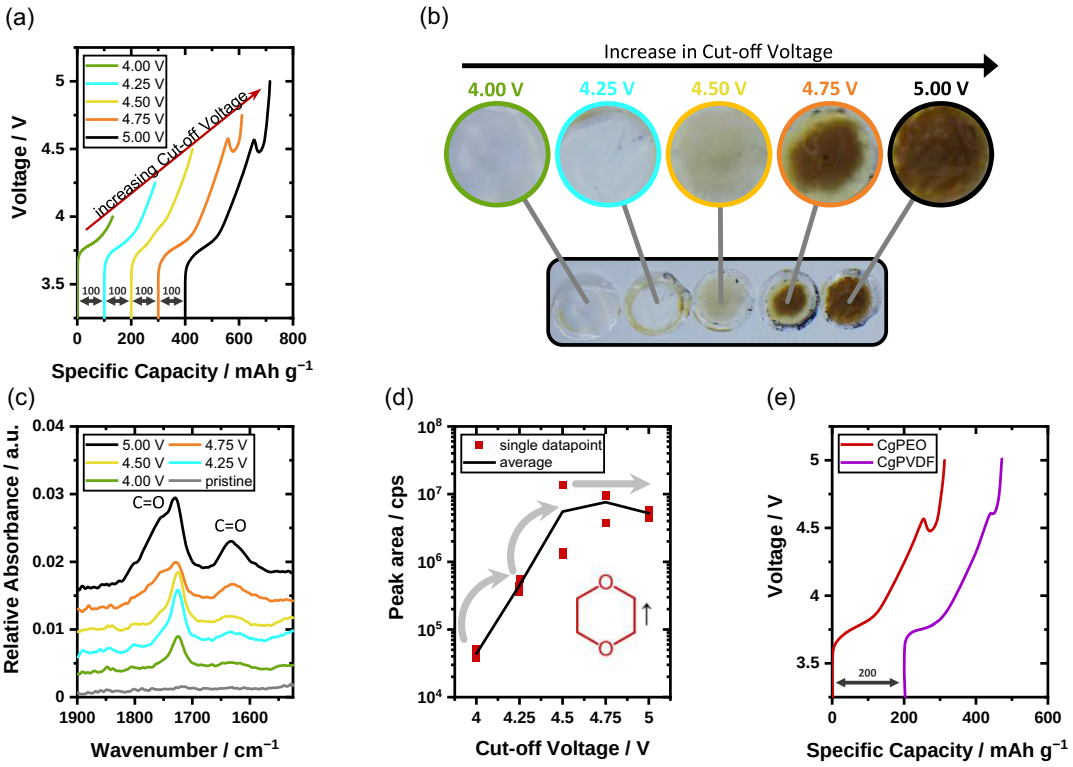

Figure 5. Degradation of NMC622||Li cells containing CgPEO and CgPVDF. a) LSAs in NMC622||Li cells containing CgPEO at 60 °C with 0.05 mA cm^{-2} and varying the cut-off voltages from 4 to 5 V; b) photographs of the corresponding electrolytes after LSA; c) IR spectra of the CgPEO electrolyte surface after LSAs from 1900 to 1525 cm^{-1}; d) SPME-GC-MS measurements of the NMC622 electrodes and CgPEO after LSAs; e) comparison of the LSAs in NMC622||Li cells containing CgPEO and CgPVDF at 60 °C with 0.05 mA cm^{-2} and a cut-off voltage of 5 V.

contribute to the cycling process of Li^+, active material is lost, decreasing cell capacity and increasing cell resistances by electrolyte and NMC degradation products.[35,36] The voltage drop and buildup of resistances of CgPEO is further evaluated by staircase cyclic amperometry coupled with impedance spectroscopy, see Figure S4, Supporting Information.

In summary, an oxidation of PEO is detected from 4.00 V on, supporting the results from LSV measurements. Therefore, the upper ESW of the CgPEO electrolyte is below the applied cut-off voltage of 4.25 V in NMC622||Li cells, supporting the replacement of PEO by PVDF-HFP to increase the ESW. Furthermore, it is shown that volatile degradation products are even formed at <4.5 V within the voltage range of high-voltage cathode materials of the 4 V category. A more detailed analysis of the degradation products aside from 1,4-dioxane, 2-methoxy-1-propanol, 1,2-ethylene glycol diformate, and 1,3,6-trioxocane will be discussed in more detail in upcoming work. Additionally, a severe degradation at ≈4.6 V, which leads to cell failure, is observed. This effect causes a rapid increase in impedance and capacity loss. As highlighted in the context of current research, the oxidation of PEO can come along with a reduction reaction, which can contribute to cell failure, e.g., NMC degradation.

While LSV and LSA measurements give first insights into general oxidative stability, during cycling the electrolytes are exposed to an oxidative environment for a much longer period of time. To compare the long-term oxidative stability of CgPEO and CgPVDF, the electrolytes are cycled in NMC622||Li cells coupled with electrochemical impedance measurement performed after each cycle. As seen in **Figure 6**a, CgPEO cells show initially a higher specific discharge capacity during cycling compared to CgPVDF cells. The initially lower specific discharge capacity of CgPVDF is related to the higher tensile strength (stiffness) of PVDF-HFP electrolytes (50 MPa) compared to PEO electrolytes (<5 MPa), decreasing the electrolyte cathode contact.[37] Furthermore, the crystallinity of PVDF-HFP lowers IL uptake in the cathode-facing region of the electrolyte, further decreasing the cathode contact.[38] Additionally, PEO (65 °C) has a much lower melting point than PVDF-HFP (135 °C), which further reduces the crystallinity and stiffness of PEO during cell operation at elevated temperatures.[38] Despite the initially higher specific discharge capacity, the CgPEO cells show rapid capacity loss compared to CgPVDF cells, which cycle more stably. The capacity loss is evaluated by the specific energy of a cell, which represents how much energy is stored in a battery cell per mass, see Equation (1). The specific energy of a cell depends on the average operating cell voltage (U_{cell}), the cathode capacity ($Q_{cathode}$), and the total cell mass (m_{cell}). While m_{cell} remains unchanged both U_{cell} and $Q_{cathode}$ decline during cycling for CgPEO cells, see Figure 6b. As seen from the voltage profiles of the 1st, 10th, and 50th cycle, the CgPEO cells gradually lose $Q_{cathode}$, which is visible by a shift of the voltage profiles to lower specific capacities. Additionally, the voltage curves of the cell charging are shifted to higher voltages, which causes the

© 2023 The Authors. Advanced Energy and Sustainability Research published by Wiley-VCH GmbH

26999412, 2023, 12, Downloaded from https://onlinelibrary.wiley.com/doi/10.1002/aesr.202300153 by Forschungszentrum Jülich GmbH Research Center, Wiley Online Library on [09/04/2024]. See the Terms and Conditions (https://onlinelibrary.wiley.com/terms-and-conditions) on Wiley Online Library for rules of use; OA articles are governed by the applicable Creative Commons License

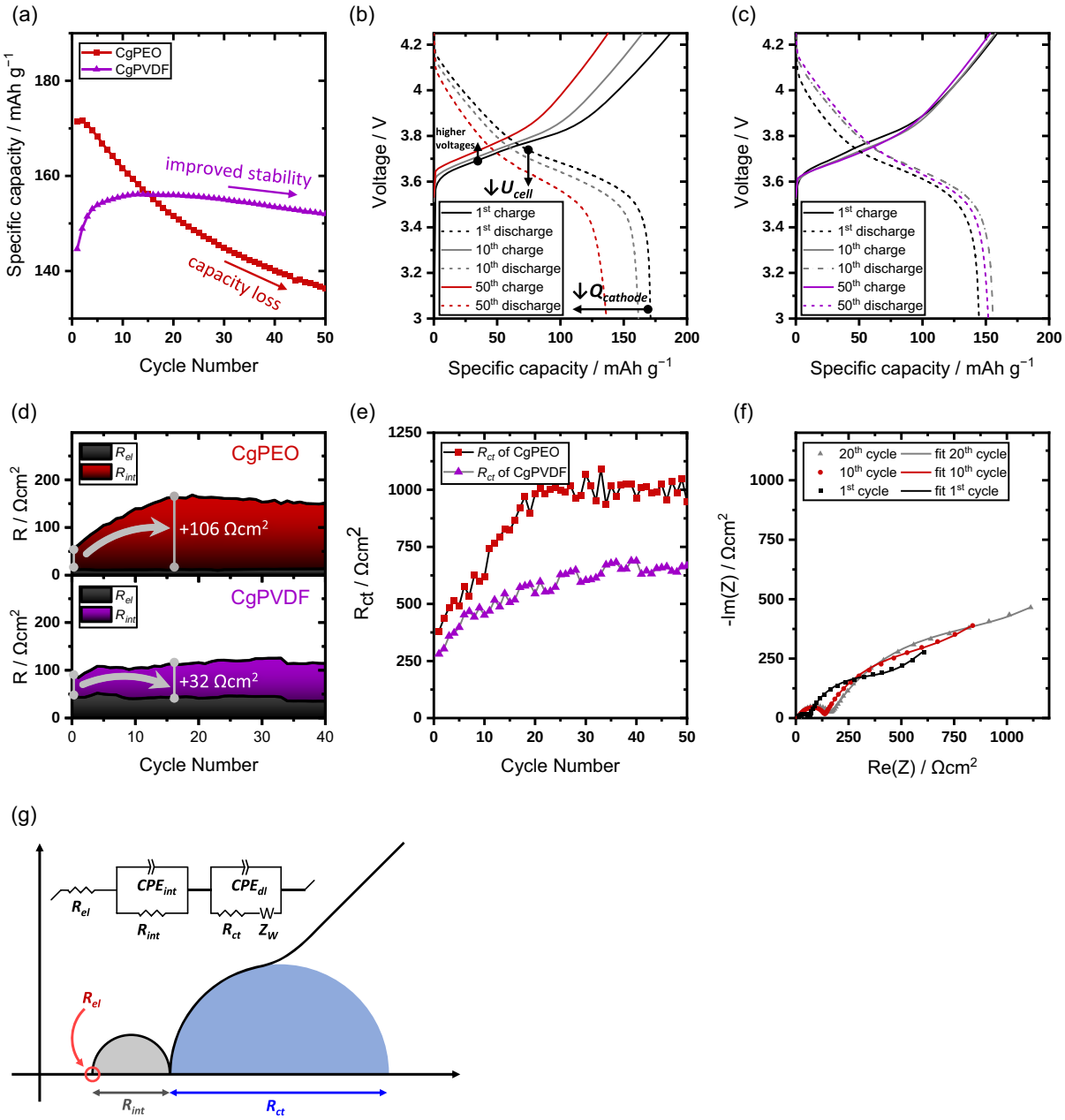

Figure 6. Comparison of the long-term cycling stability of NMC622||Li cells with CgPEO and CgPVDF coupled with an impedance measurement at 60 °C. a) Specific discharge capacity over cycle number with 0.05 mA cm^{-2} and cut-off voltages from 3.00 to 4.25 V; b) voltage profile for CgPEO-based cells over the specific capacity of the 1st, 10th, and 50th cycle; c) voltage profile for CgPVDF-based cells over the specific capacity of the 1st, 10th, and 50th cycle; d) development of R_{el} and R_{int} over cycle number; e) development of R_{ct} over cycle number; f) Nyquist plots of CgPEO after the 1st, 10th, and 20th cycle; g) schematic equivalent circuit used to fit the Nyquist plots.

cut-off voltage to be reached with a lower SOC also decreasing the available $Q_{cathode}$ within the set voltage range. Furthermore, U_{cell} declines, which is indicated by a shift of the voltage profiles of the cell discharging to lower voltages. For the CgPVDF cells, the specific discharge capacity and therefore $Q_{cathode}$ do not decline from the 1st to the 50th cycle, see Figure 6c. Also, no major increase in U_{cell} is noticeable as the voltage profiles of the cell discharging do not decline but even slightly increase from the 1st cycle.

$$\text{Specific Energy} = \frac{U_{cell} \times U_{cathode}}{m_{cell}} \quad (1)$$

Specific energy/Wh kg^{-1}
U_{cell} – average operating cell voltage/V
$Q_{cathode}$ – cathode capacity/Ah
m_{cell} – total cell mass/kg

To understand the major differences in the cycling of CgPEO compared to CgPVDF in more detail, impedance spectroscopy is

© 2023 The Authors. Advanced Energy and Sustainability Research published by Wiley-VCH GmbH

26999412, 2023, 12, Downloaded from https://onlinelibrary.wiley.com/doi/10.1002/aesr.202300153 by Forschungszentrum Jülich GmbH Research Center, Wiley Online Library on [09/04/2024]. See the Terms and Conditions (https://onlinelibrary.wiley.com/terms-and-conditions) on Wiley Online Library for rules of use; OA articles are governed by the applicable Creative Commons License

used. Since a decomposition comes along with a change in cell chemistry, the ion transport through the cell materials of the cell is affected. The impediment for ion transport is caused by resistances/impedances in the cell, which are distinguished by the resistance of the electrolyte (R_{el}), the resistances within the electrodes (R_{ct}), and the resistances of the electrode|electrolyte interfaces/interphases (I&I) (R_{int}). To fit the data, a $R_{el} + (R_{int}/CPE_{int}) + (CPE_{dl}/R_{ct} + Z_W)$ circuit build of the elements resistor (R), constant phase element (CPE), and transport (often denoted as Warburg) element (Z_W) is used, see Figure 6f,g. The parallel connection of the R_{int}/CPE_{int} element represents the I&I, with R_{int} being the resistance for charge transfer and CPE_{int} represents the capacitive behavior of the ionic double layer at the electrode|electrolyte I&I. To represent transport phenomena in the low-frequency region like ion diffusion in the electrolyte or Li^+ intercalation in the NMC particles, a $CPE_{dl}/R_{ct} + Z_W$ element is added. CPE_{dl} represents the capacitive behavior of the ionic double layer at the electrolyte|NMC interface, R_{ct} represents the charge transfer resistance, and Z_W is the ion diffusion inside of the electrolyte and NMC. As shown in Figure 6d, R_{el} (gray area) remains stable for both electrolytes over 50 cycles with an average of 12 $\Omega\,cm^2$ (CgPEO) and 42 $\Omega\,cm^2$ (CgPVDF). The bulk electrolyte therefore maintains its ionic conductivity showing no effects by aging or degradation. The higher resistance for CgPVDF can be related to a lower IL uptake and lower Li salt dissociation of the PVDF-HFP region, causing a region of higher resistance increasing the total R_{el}.[27,39] For the R_{int} development, a notable difference between CgPEO and CgPVDF is observed, see Figure 6d. After the 20th cycle, R_{int} increases by +106 $\Omega\,cm^2$ for CgPEO and +32 $\Omega\,cm^2$ for CgPVDF. The major increase for CgPEO indicates the development of a thick CEI at the CgPEO|NMC I&I. During the oxidation of PEO, the $M^{+IV}O_2$ are reduced by oxygen loss to form metal(II)-oxides ($M^{+II}O$).[40,41] Because M^{+II}Os at the surface of NMC particles limit the ion diffusion by forming additional interphase, the total R increases, which results in a decline in U_{cell}.[30,42,43] Furthermore, M^{+II}Os do not participate in the redox process of lithiation and delithiation and the transition to M^{+II}Os is thermodynamically favorable, therefore active cathode material is lost, which reduces $Q_{cathode}$.[40] In addition, by the oxidative ester formation of PEO H^+ is formed, which reacts with $TFSI^-$ to form HTFSI that is capable of dissolution of the NMC-cations further eroding the interface by ongoing cathode degradation finally resulting in a reduction of $Q_{cathode}$.[25,41,44] Additionally, the R_{ct} evolution is compared, see Figure 6e. Hereby, it has to be noted that R_{ct} depends on the charging state of the NMC||Li cells.[45,46] While R_{ct} becomes small at high charging states, it rises during discharge. Therefore, for comparison, the R_{ct} values after complete discharge are compared. After 40 cycles a plateau is reached for R_{ct} for both cells. The average R_{ct} (41–50th cycle) is 650 $\Omega\,cm^2$ for CgPVDF and 1 000 $\Omega\,cm^2$ for CgPEO, respectively. The higher R_{ct} of CgPEO compared to CgPVDF indicates that a more intensive deterioration of the NMC622 particles is present, which increases the resistance for ion conduction within the cathode material.[45,47,48]

In summary, exchanging PEO by PVDF-HFP at the cathode-facing side of the electrolyte improves the capacity retention in NMC622||Li cells. CgPEO suffers from a decline of U_{cell} as well as $Q_{cathode}$. The impedance measurement revealed a major difference in the development of R_{ct} and R_{int} for CgPEO and CgPVDF. The improved oxidative stability of CgPVDF resulted in a decreased formation of R in the cell.

2.2. Electrochemical Performance of Cells with CgPVDF versus CgPVDF+

Despite the benefits of CgPVDF compared to CgPEO, the low ionic conductivity of the electrolyte as observed by the high R_{el} limits electrochemical performance. In comparison to PEO with its EO chain, Li-ion coordinating oxygen groups are absent in PVDF-HFP.[37,39] Therefore, the Li salt dissociation in PVDF-HFP-based SPEs is limited. To improve ionic conductivity, two strategies could be applied. First, the amount of charge carriers can be increased. As observed by Gonçalves et al. the ionic conductivity of a PVDF-HFP-based SPE is improved with increasing LiTFSI content.[49] By creating a polymer-in-salt-electrolyte with a LiTFSI content of 80%, the Li salt is precipitated, enabling high ionic conductivity by percolation networks.[37,39] Second, the mobility of charge carriers can be increased by higher IL contents. As discussed by Kim et al. the ionic conductivity of a TSPE is increased with IL content.[19] While the first approach is suitable for SPEs, in IL-containing TSPEs the formation of ion-clusters decreases the performance.[50] Therefore, the second approach is followed to improve the ionic conductivity of CgPVDF. By increasing the Pyr_{14}TFSI content in CgPVDF from a ratio of 10:2:1 ($EO_{equiv.}$:Pyr_{14}TFSI:LiTFSI) to 10:4:1 (CgPVDF+) the R_{el} is reduced, see Figure S17, Supporting Information. Hereby the resulting CgPVDF+ does maintain a high mechanical strength originated by the Cg domain. As shown by Zhang et al. the elastic modulus of a Cg-reinforced TSPE (121 MPa) is much higher than the pure TSPE (0.3 MPa), which indicates that the mechanical strength is mainly determined by the Cg. The electrochemical performances of CgPVDF and CgPVDF+ are evaluated in Li||Li cells.

The areal capacity utilization is determined by galvanostatic discharge polarization, see **Figure 7**a. A constant current of 0.1 mA cm^{-2} is applied and the voltage is monitored over the areal capacity. A rapid voltage drop is visible for both samples at 45 mAh cm^{-2} (CgPVDF) and 42 mAh cm^{-2} (CgPVDF+) indicating a short-circuit caused by HSAL growth through the electrolyte. While the areal capacity utilization is lower than for CgPEO (53 mAh cm^{-2}), it is higher than a pure TSPE (<5 mAh cm^{-2}) indicating that the Cg membrane dominates the HSAL-preventing properties rather than the ternary electrolyte composition, see **Table 1**.[20]

To evaluate the performance of the electrolytes, the limiting diffusion current rate of the electrolyte is determined by voltammetry ($j_{lim,\ pot}$) and amperometry ($j_{lim,\ gal}$) described elsewhere.[51] In this case, j_{lim} determines the maximal amount of charge, which is transported through the electrolyte (ion diffusion) between the Li metal electrodes. To determine $j_{lim,\ gal}$, charge pulses of $\geq$0.8 mA cm^{-2} are applied till the cut-off voltage of 1 V is reached. Due to a faster depletion of Li^+ at the Li|electrolyte interface with increasing current density, the time till the cut-off voltage is reached decreases.[51] As described by Wetjen et al. $j_{lim,\ gal}$ can be derived from the x-axis intercept of the inverse charge density over the current density plot, which can be

© 2023 The Authors. Advanced Energy and Sustainability Research published by Wiley-VCH GmbH

26999412, 2023, 12, Downloaded from https://onlinelibrary.wiley.com/doi/10.1002/aesr.202300153 by Forschungszentrum Jülich GmbH Research Center, Wiley Online Library on [09/04/2024]. See the Terms and Conditions (https://onlinelibrary.wiley.com/terms-and-conditions) on Wiley Online Library for rules of use; OA articles are governed by the applicable Creative Commons License

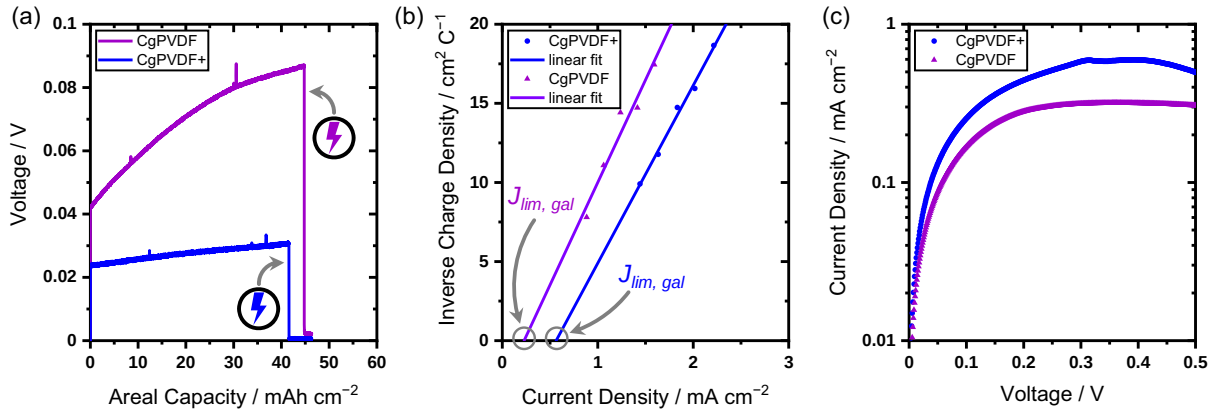

Figure 7. Electrochemical performance of Li||Li cells with CgPVDF and CgPVDF+ performed at 60 °C. a) Galvanostatic discharge polarization with 0.1 mA cm^{-2} until short circuit; b) inverse charge density versus current density; c) LSV with a scan rate of 0.01 mV s^{-1}.

Table 1. Comparison of j_{lim} and capacity utilization of Li||Li cells with CgPEO, CgPVDF, and CgPVDF+ at 60 °C.

	$j_{lim, gal}$ [mA cm^{-2}]	$j_{lim, pot}$ [mA cm^{-2}]	Capacity utilization [mAh cm^{-2}]
CgPEO	N/A	0.36[20]	53[20]
CgPVDF	0.29 ± 0.05	0.30 ± 0.03	45
CgPVDF+	0.61 ± 0.05	0.60 ± 0.05	42

determined from the depletion time and the current density.[51] An average $j_{lim, gal}$ of (0.29 ± 0.05) mA cm^{-2} for CgPVDF and (0.61 ± 0.05) mA cm^{-2} for CgPVDF+ is determined, see Figure 7b. Furthermore, the $j_{lim, pot}$ is determined by LSV applying a scan rate of 0.01 mV s^{-1}, see Figure 7c. The maximal current density measured of (0.30 ± 0.03) mA cm^{-2} (CgPVDF) and (0.60 ± 0.05) mA cm^{-2} (CgPVDF+) represents $j_{lim, pot}$. CgPVDF shows a lower j_{lim} compared to CgPEO which agrees with the assumption of a higher R_{el} hindering ion diffusion through the electrolyte. CgPVDF+ shows a higher j_{lim} compared to CgPVDF with an improving electrolyte performance from 0.3 to 0.6 mA cm^{-2}. The applied methods show comparable j_{lim} values.

2.3. Thermal Stability of CgPVDF+

The thermal stability of CgPVDF+ and its components is determined by TGA, see **Figure 8**. A noticeable mass (m) in relation to the initial mass (m/m_0) is lost in CgPVDF+ for temperatures (T) ≥330 °C, see Figure 8a. The differential of the mass loss per temperature ($|dm\,dT^{-1}|$) indicates two major mass loss regions: PEO and LiTFSI degrade at ≈350 °C and Cg, PVDF-HFP and $Pyr_{14}TFSI$ degrade at ≈450 °C, compare Figure 8b. The addition of PVDF-HFP does not limit the overall thermal stability and is therefore comparable to CgPEO. Overall CgPVDF+ has a thermal stability of >300 °C.

2.4. Cycling Performance of Cells with CgPVDF+

The long-term cycling performance of NMC622||Li and LFP||Li cells with CgPVDF+ is given in **Figure 9** and **10**. In the 1st cycle, the voltage of NMC622||Li cells is higher compared to the subsequent cycles, which is caused by the artificial solid electrolyte interphase (SEI) increasing the I&I resistance.[52] Afterward, fresh Li is plated reducing the overvoltage and the voltage profiles do not change significantly during cycling. The specific discharge

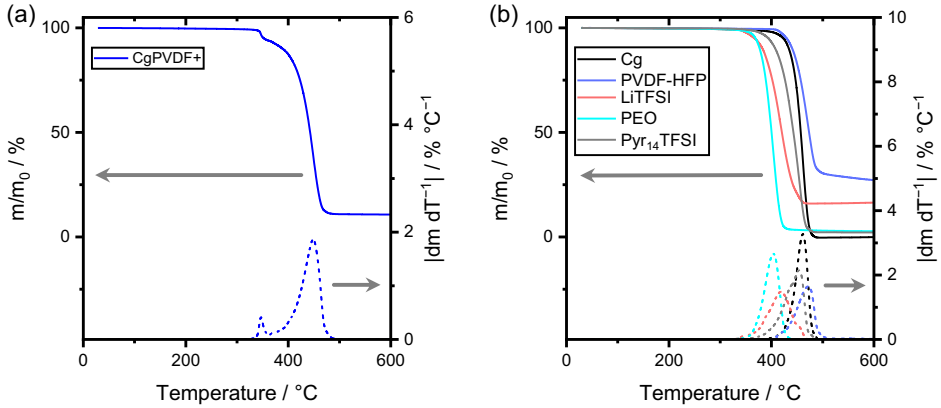

Figure 8. TGA from 30 to 600 °C, with a scan rate of 10 K min^{-1} under inert gas of a) CgPVDF+ and b) the individual components Cg, PVDF-HFP, LiTFSI, PEO, and $Pyr_{14}TFSI$.

© 2023 The Authors. Advanced Energy and Sustainability Research published by Wiley-VCH GmbH

26999412, 2023, 12, Downloaded from https://onlinelibrary.wiley.com/doi/10.1002/aesr.202300153 by Forschungszentrum Jülich GmbH Research Center, Wiley Online Library on [09/04/2024]. See the Terms and Conditions (https://onlinelibrary.wiley.com/terms-and-conditions) on Wiley Online Library for rules of use; OA articles are governed by the applicable Creative Commons License

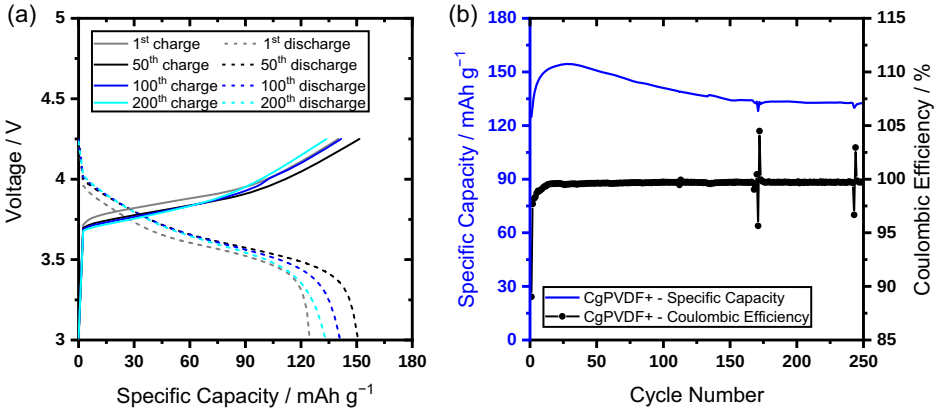

Figure 9. Long-term cycling performance of NMC622||Li cells with CgPVDF+ at 60 °C with 0.1 mA cm^{-2} and cut-off voltages from 3.00 to 4.25 V. a) Voltage profile over specific capacity of the 1st, 50th, 100th, and 200th cycle; b) specific discharge capacity and Coulombic efficiency over cycle number.

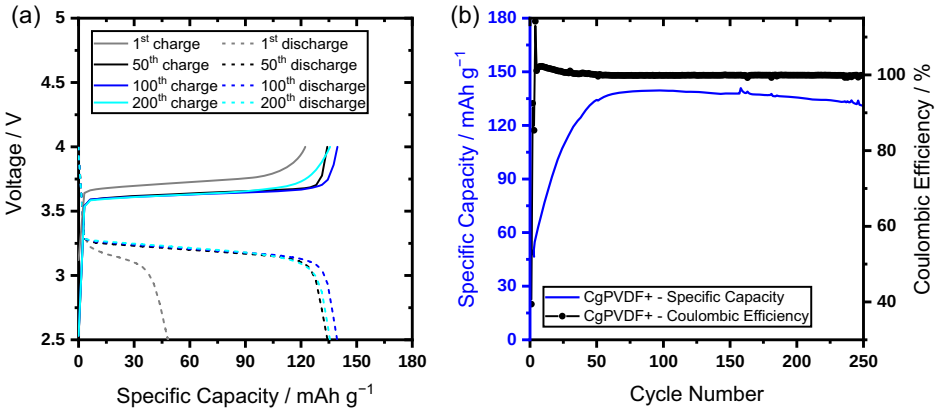

Figure 10. Long-term cycling performance of LFP||Li cells with CgPVDF+ at 60 °C with 0.1 mA cm^{-2} and cut-off voltages from 2.50 to 4.00 V. a) Voltage profile over specific capacity of the 1st, 50th, 100th, and 200th cycle; b) specific discharge capacity and Coulombic efficiency over cycle number.

capacity remains at a high value with a capacity retention of 87% after 150 cycles and 86% after 250 cycles (compared to the maximal specific discharge capacity), indicating a low fading from cycle 150 onward. Furthermore, the Coulombic efficiency increases from 89% of the 1st cycle to an average of 99.7% (150–250th cycle) indicating a stable reversible cycling. When compared to CgPEO, CgPVDF+ provides greater capacity retention, compare Figure S5, Supporting Information. Further information in regards of the rate capability and development of impedances in NMC622||Li cells with CgPVDF+ is in the Supporting Information, see Figure S6 and S7, Supporting Information.

To show that CgPVDF+ is suitable as an electrolyte toward different types of cathodes, it is also cycled in a LFP||Li cell set-up. LFP gained attention due to its low cost and low environmental impact.[53] Similar to a NMC622||Li cell set-up also in LFP||Li cells the first cycle shows an increased overvoltage compared to the subsequent cycles, see Figure 10a. The Coulombic efficiency is 39% in the 1st cycle and increases rapidly in the subsequent cycles, see Figure 10b. From there the Coulombic efficiency remains at a high level of 99.9% (150–250th cycle). The specific discharge capacity is at a high value with a capacity retention of 94% after 250 cycles.

In summary, the application of the CgPVDF+ electrolyte in NMC622||Li cells shows a major improvement in capacity retention (>90% after 50 cycles) when compared to CgPEO (<80% after 50 cycles). The capacity retention of NMC622||Li and LFP||Li cells with CgPVDF+ are further compared to other electrolyte systems, see Table S1, Supporting Information. In comparison to SPEs as well as TSPEs, the capacity retention of CgPVDF+-based cells is higher. When compared to liquid electrolytes, CgPVDF+-based cells provide comparable or lower capacity retention.

3. Conclusion

In a previous publication by Zhang et al. the implementation of Cg into a PEO-based TSPE reduced the risk of cell failure by short circuit. However, as shown in literature, PEO is not stable when cycled toward high-voltage cathode materials limiting its application.[40] In our work, it is shown that PEO is degraded at ≥3.8 V. From 4.00 V, it is oxidized by the formation of carbonyl groups and volatile degradation products, like 1,4-dioxane. As a result, a fast capacity fading is observed in NMC622||Li cells. As an alternative, a multilayer electrolyte is presented in this work. A Cg

© 2023 The Authors. Advanced Energy and Sustainability Research published by Wiley-VCH GmbH

26999412, 2023, 12, Downloaded from https://onlinelibrary.wiley.com/doi/10.1002/aesr.202300153 by Forschungszentrum Jülich GmbH Research Center, Wiley Online Library on [09/04/2024]. See the Terms and Conditions (https://onlinelibrary.wiley.com/terms-and-conditions) on Wiley Online Library for rules of use; OA articles are governed by the applicable Creative Commons License

separator is coated with two different electrolytes to customize it toward the different requirements of NMC622 cathode and the Li metal anode. Hereby, the HSAL-preventing properties toward the Li anode of CgPEO are taken on. By exchanging PEO with PVDF-HFP on the cathode-facing side of the electrolyte, oxidative PEO degradation is avoided. PVDF-HFP-based ternary electrolyte CgPVDF+ enables a high voltage stability of up to 4.75 V at the electrolyte|cathode interface. Furthermore, the multilayer approach maintains a temperature stability of >300 °C and allows for a flexible and durable thin membrane (≤50 μm). The presented CgPVDF+ electrolyte enables a high Coulombic efficiency during cycling up to 99.7% in NMC622||Li cells and 99.9% in LFP||Li cells. Moreover, a great capacity retention of 86% after 250 cycles in NMC622||Li cells and 94% after 250 cycles in LFP||Li cells.

Supporting Information

Supporting Information is available from the Wiley Online Library or from the author.

Acknowledgements

The authors thank the Ministry for Culture and Science of North Rhine Westphalia (Germany) for funding this work within the International Graduate School for Battery Chemistry, Characterization, Analysis, Recycling, and Application (BACCARA).

Open Access funding enabled and organized by Projekt DEAL.

Conflict of Interest

The authors declare no conflict of interest.

Author Contributions

L.H. performed the synthesis of electrolytes, FT-IR measurement, LSM measurement, cell assembly, electrochemical measurements, and evaluation of data. The SPME-GC-MS measurements were performed and evaluated by J.M. The SEM measurements were performed by S.S. The TGA measurements were performed by D.B. M.W., and P.B. supervised the work. L.H. wrote the first version of the manuscript, which was supplemented through contributions of J.M., V.K., P.B., S.N., and M.W.

Data Availability Statement

The data that support the findings of this study are available from the corresponding author upon reasonable request.

Keywords

coated separators, ionic liquids, lithium metals, multilayer electrolytes, polyethylene oxide

Received: August 2, 2023
Revised: August 16, 2023
Published online: October 6, 2023

[1] A. Kalair, N. Abas, M. S. Saleem, A. R. Kalair, N. Khan, *Energy Storage* **2021**, *3*, e135.
[2] J. Deng, C. Bae, A. Denlinger, T. Miller, *Joule* **2020**, *4*, 511.
[3] A. G. Olabi, C. Onumaegbu, T. Wilberforce, M. Ramadan, M. A. Abdelkareem, A. H. Al-Alami, *Energy* **2021**, *214*, 118987.
[4] S. Chu, A. Majumdar, *Nature* **2012**, *488*, 294.
[5] S. Koohi-Fayegh, M. A. Rosen, *J. Energy Storage* **2020**, *27*, 101047.
[6] X. Sun, Z. Li, X. Wang, C. Li, *Energies* **2020**, *13*, 90.
[7] D. Lin, Y. Liu, Y. Cui, *Nat. Nanotechnol.* **2017**, *12*, 194.
[8] Z. Wu, K. Sun, Z. Wang, *Batteries* **2022**, *8*, 246.
[9] J. Liu, Z. Bao, Y. Cui, E. J. Dufek, J. B. Goodenough, P. Khalifah, Q. Li, B. Y. Liaw, P. Liu, A. Manthiram, Y. S. Meng, V. R. Subramanian, M. F. Toney, V. V. Viswanathan, M. S. Whittingham, J. Xiao, W. Xu, J. Yang, X.-Q. Yang, J.-G. Zhang, *Nat. Energy* **2019**, *4*, 180.
[10] J. W. Choi, D. Aurbach, *Nat. Rev. Mater.* **2016**, *1*, 16013.
[11] P. V. Chombo, Y. Laoonual, *J. Power Sources* **2020**, *478*, 228649.
[12] Y. An, X. Han, Y. Liu, A. Azhar, J. Na, A. K. Nanjundan, S. Wang, J. Yu, Y. Yamauchi, *Small* **2022**, *18*, 2103617.
[13] X.-B. Cheng, R. Zhang, C.-Z. Zhao, Q. Zhang, *Chem. Rev.* **2017**, *117*, 10403.
[14] Z. Cheng, T. Liu, B. Zhao, F. Shen, H. Jin, X. Han, *Energy Storage Mater.* **2021**, *34*, 388.
[15] S. Qian, H. Chen, Z. Wu, D. Li, X. Liu, Y. Tang, S. Zhang, *Batteries Supercaps* **2021**, *4*, 39.
[16] J. Wu, L. Yuan, W. Zhang, Z. Li, X. Xie, Y. Huang, *Energy Environ. Sci.* **2021**, *14*, 12.
[17] A. Ahniyaz, I. de Meatza, A. Kvasha, O. Garcia-Calvo, I. Ahmed, M. F. Sgroi, M. Giuliano, M. Dotoli, M.-A. Dumitrescu, M. Jahn, N. Zhang, *Adv. Appl. Energy* **2021**, *4*, 100070.
[18] D.-H. Liu, Z. Bai, M. Li, A. Yu, D. Luo, W. Liu, L. Yang, J. Lu, K. Amine, Z. Chen, *Chem. Soc. Rev.* **2020**, *49*, 5407.
[19] G. T. Kim, G. B. Appetecchi, M. Carewska, M. Joost, A. Balducci, M. Winter, S. Passerini, *J. Power Sources* **2010**, *195*, 6130.
[20] M. Zhang, A. L. Gui, W. Sun, J. Becking, O. Riedel, X. He, D. Berghus, V. Siozios, D. Zhou, T. Placke, M. Winter, P. Bieker, *J. Electrochem. Soc.* **2019**, *166*, A2142.
[21] X. Ji, Y. Zhang, M. Cao, Q. Gu, H. Wang, J. Yu, Z.-H. Guo, X. Zhou, *J. Adv. Ceram.* **2022**, *11*, 835.
[22] J. Li, F. Li, L. Zhang, H. Zhang, U. Lassi, X. Ji, *Green Chem. Eng.* **2021**, *2*, 253.
[23] L. Herbers, V. Küpers, M. Winter, P. Bieker, *RSC Adv.* **2023**, *13*, 17947.
[24] D. R. Gallus, R. Wagner, S. Wiemers-Meyer, M. Winter, I. Cekic-Laskovic, *Electrochim. Acta* **2015**, *184*, 410.
[25] K. Nie, X. Wang, J. Qiu, Y. Wang, Q. Yang, J. Xu, X. Yu, H. Li, X. Huang, L. Chen, *ACS Energy Lett.* **2020**, *5*, 826.
[26] M. Winter, B. Barnett, K. Xu, *Chem. Rev.* **2018**, *118*, 11433.
[27] M. A. Cabañero Martínez, N. Boaretto, A. J. Naylor, F. Alcaide, G. D. Salian, F. Palombarini, E. Ayerbe, M. Borras, M. Casas-Cabanas, *Adv. Mater.* **2022**, *12*, 2201264.
[28] M. Metzger, C. Marino, J. Sicklinger, D. Haering, H. A. Gasteiger, *J. Electrochem. Soc.* **2015**, *162*, A1123.
[29] F. Horsthemke, A. Friesen, X. Mönnighoff, Y. P. Stenzel, M. Grützke, J. T. Andersson, M. Winter, S. Nowak, *RSC Adv.* **2017**, *7*, 46989.
[30] J. Qiu, X. Liu, R. Chen, Q. Li, Y. Wang, P. Chen, L. Gan, S.-J. Lee, D. Nordlund, Y. Liu, X. Yu, X. Bai, H. Li, L. Chen, *Adv. Funct. Mater.* **2020**, *30*, 1909392.
[31] X. Yang, M. Jiang, X. Gao, D. Bao, Q. Sun, N. Holmes, H. Duan, S. Mukherjee, K. Adair, C. Zhao, J. Liang, W. Li, J. Li, Y. Liu, H. Huang, L. Zhang, S. Lu, Q. Lu, R. Li, C. V. Singh, X. Sun, *Energy Environ. Sci.* **2020**, *13*, 1318.
[32] L. Costa, A. M. Gad, G. Camino, G. G. Cameron, M. Y. Qureshi, *Macromolecules* **1992**, *25*, 5512.

© 2023 The Authors. Advanced Energy and Sustainability Research published by Wiley-VCH GmbH

26999412, 2023, 12, Downloaded from https://onlinelibrary.wiley.com/doi/10.1002/aesr.202300153 by Forschungszentrum Jülich GmbH Research Center, Wiley Online Library on [09/04/2024]. See the Terms and Conditions (https://onlinelibrary.wiley.com/terms-and-conditions) on Wiley Online Library for rules of use; OA articles are governed by the applicable Creative Commons License

[33] E. Finocchio, C. Cristiani, G. Dotelli, P. G. Stampino, L. Zampori, *Vib. Spectrosc.* **2014**, *71*, 47.
[34] G. Homann, L. Stolz, J. Nair, I. C. Laskovic, M. Winter, J. Kasnatscheew, *Sci. Rep.* **2020**, *10*, 4390.
[35] R. Jung, P. Strobl, F. Maglia, C. Stinner, H. A. Gasteiger, *J. Electrochem. Soc.* **2018**, *165*, A2869.
[36] R. Jung, M. Metzger, F. Maglia, C. Stinner, H. A. Gasteiger, *J. Electrochem. Soc.* **2017**, *164*, A1361.
[37] Y. Wu, Y. Li, Y. Wang, Q. Liu, Q. Chen, M. Chen, *J. Energy Chem.* **2022**, *64*, 62.
[38] L. Long, S. Wang, M. Xiao, Y. Meng, *J. Mater. Chem. A* **2016**, *4*, 10038.
[39] J. Mindemark, M. J. Lacey, T. Bowden, D. Brandell, *Prog. Polym. Sci.* **2018**, *81*, 114.
[40] H. Zhang, J. Zhang, J. Ma, G. Xu, T. Dong, G. Cui, *Electrochem. Energy Rev.* **2019**, *2*, 128.
[41] M. Yi, J. Li, M. Wang, X. Fan, B. Hong, Z. Zhang, Z. Zhang, H. Jiang, A. Wang, Y. Lai, *Energy Storage Mater.* **2023**, *54*, 579.
[42] J. Li, Y. Ji, H. Song, S. Chen, S. Ding, B. Zhang, L. Yang, Y. Song, F. Pan, *Nano Micro Lett.* **2022**, *14*, 191.
[43] T. Li, X.-Z. Yuan, L. Zhang, D. Song, K. Shi, C. Bock, *Electrochem. Energy Rev.* **2020**, *3*, 43.
[44] R. Huang, Y. Ding, F. Zhang, W. Jiang, C. Zhang, P. Yan, M. Ling, H. Pan, *J. Energy Chem.* **2022**, *75*, 504.
[45] V. Charbonneau, A. Lasia, G. Brisard, *J. Electroanal. Chem.* **2020**, *875*, 113944.
[46] N. Meddings, M. Heinrich, F. Overney, J.-S. Lee, V. Ruiz, E. Napolitano, S. Seitz, G. Hinds, R. Raccichini, M. Gaberšček, J. Park, *J. Power Sources* **2020**, *480*, 228742.
[47] Y. Li, J. Guo, K. Pedersen, L. Gurevich, D.-I. Stroe, *J. Energy Chem.* **2023**, *80*, 237.
[48] C. Busà, M. Belekoukia, M. J. Loveridge, *Electrochim. Acta* **2021**, *366*, 137358.
[49] R. Gonçalves, D. Miranda, A. M. Almeida, M. M. Silva, J. M. Meseguer-Dueñas, J. G. Ribelles, S. Lanceros-Méndez, C. M. Costa, *Sustainable Mater.Technol.* **2019**, *21*, e00104.
[50] R.-S. Kühnel, A. Balducci, *J. Phys. Chem. C* **2014**, *118*, 5742.
[51] M. Wetjen, G.-T. Kim, M. Joost, M. Winter, S. Passerini, *Electrochim. Acta* **2013**, *87*, 779.
[52] J. Wellmann, J.-P. Brinkmann, B. Wankmiller, K. Neuhaus, U. Rodehorst, M. R. Hansen, M. Winter, E. Paillard, *ACS Appl. Mater. Interfaces* **2021**, *13*, 34227.
[53] Y. Mekonnen, A. Sundararajan, A. I. Sarwat, in *SoutheastCon*, IEEE, New York City, USA **2016**, p. 1.

© 2023 The Authors. Advanced Energy and Sustainability Research published by Wiley-VCH GmbH

26999412, 2023, 12, Downloaded from https://onlinelibrary.wiley.com/doi/10.1002/aesr.202300153 by Forschungszentrum Jülich GmbH Research Center, Wiley Online Library on [09/04/2024]. See the Terms and Conditions (https://onlinelibrary.wiley.com/terms-and-conditions) on Wiley Online Library for rules of use; OA articles are governed by the applicable Creative Commons License